DEVELOPMENT OF AN EFFECTIVE VISCOSITY MODEL FOR NANO- AND MICROPARTICLE SUSPENSIONS

by

Jon Langston

Submitted in partial fulfillment of the
requirements for Departmental Honors in
the Department of Engineering
Texas Christian University
Fort Worth, Texas

May 4, 2015

DEVELOPMENT OF AN EFFECTIVE VISCOSITY MODEL

FOR NANO- AND MICROPARTICLE SUSPENSIONS

Project Approved:

Supervising Professor: Efstathios Michaelides, Ph.D.

Department of Engineering

Robert Bittle, Ph.D.

Department of Engineering

Efton Park, Ph.D.

Department of Mathematics

ABSTRACT

The purpose of this project was to develop a mathematical model relating the effective viscosity of a microparticulate suspension and the viscosity of the suspension's base fluid as a function of volumetric ratio and temperature. This was done by measuring the viscosity of water-kaolinite mixtures of 1%, 2%, 3%, and 5% volumetric ratio across temperatures ranging from 15 to 80 °C (288 to 353 K) using capillary viscometers. The raw data was then reduced in order to determine coefficients for a correlation modeled after the Einstein expression for effective viscosity. The resulting coefficients exhibited an exponential decay as temperature increased, and increased viscosity at higher concentrations. Utilizing these coefficients, an effective viscosity model as a function of temperature was developed for each of the four concentration levels. The predicted values of effective viscosity from these models agree with the measured viscosity values within 3.5% across all temperatures measured.

TABLE OF CONTENTS

DEFINITION OF VARIABLES

A: coefficient in model for K [dimensionless]

B: coefficient in model for K [dimensionless]

C: coefficient in model for K [K^{-1}]

K: coefficient of ϕ in modified Einstein expression for effective viscosity [dimensionless]

m_f: fluid (water) mass [kg]

m_s: solid (kaolinite) mass [kg]

T: temperature [K]

t: time [s]

u: local fluid velocity [m/s]

y: distance between local fluid and channel boundary [m]

μ_e: effective dynamic viscosity of mixture [Pa*s]

μ_f: fluid dynamic viscosity [Pa*s]

ν: kinematic viscosity [m^2/s]

τ: shear stress [Pa]

ρ_e: effective density of mixture [kg/m^3]

ρ_f: fluid density [kg/m^3]

ρ_s: solid density [kg/m^3]

ϕ: volumetric ratio of particles [dimensionless]

LIST OF FIGURES AND TABLES

INTRODUCTION

Nanofluids are suspensions of nanoparticles, typically 1-100 nm in diameter, often using a common engineering fluid such as water or oil [1]. These mixtures carry great potential for use in heat transfer applications such as power systems and microelectronics, due to the enhancement of thermophysical properties such as conductivity and heat transfer coefficient over those of the base fluid. As a result, nanofluids have been the focus of rapidly increasing amounts of research over the past two decades. Despite the volume of work, however, many study results still conflict with one another on a regular basis, and substantiated models and theories on nanofluid properties and behaviors are few and far-between. Although it is presumed that great benefit could result from use of nanofluids, they must be better understood before conclusive decisions and useful engineering products can be made.

Rheological behaviors, those pertaining to flow characteristics, are one of the primary sources of uncertainty in understanding nanofluids. With the introduction of small solid particles, additional shear forces are generated between solid particles and the liquid, causing the effective viscosity of the mixture to increase. Numerous studies into the viscous behavior of these mixtures have been undertaken; however, there is no single model wholly agreed upon by the scientific community. The aim of this project is to characterize these changes in viscosity in terms of temperature and volumetric fraction of particles for a distilled water-kaolinite mixture.

FLUID FLOW AND VISCOSITY

Base Fluid

The primary objective of this project is to measure the viscosity of particulate suspensions. To do so, the flow behavior of the base fluid must first be understood. As a fluid flows past a solid boundary, shear forces between the fluid and the solid cause a non-uniform velocity profile to develop in the fluid. Figure 1 displays this behavior in the case of Couette flow. The dynamic viscosity is defined as the ratio of shear stress within a fluid to the rate of shear, the derivative of the velocity profile, as follows:

$$\mu_f = \frac{\tau}{\partial u / \partial y} \quad . \tag{1}$$

The kinematic viscosity (ν), the parameter measured in the experimental portion of this work, is the ratio of dynamic viscosity to the fluid density, μ/ρ [2].

It is useful to define two types of fluid, Newtonian and non-Newtonian, according to viscous behavior. For Newtonian fluids at a given temperature, the relationship between shear stress and velocity gradient is a linear one, giving μ_f a constant value. This value typically decreases with increasing temperature due to altered molecular interaction reducing the shear stress present. Conversely, non-Newtonian fluids are those which deviate from the properties of Newtonian fluids in any way, typically with viscosity dependent on the rate of shear. The vast majority of nano-

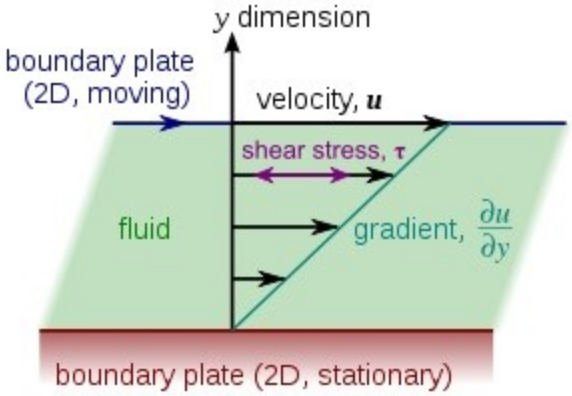

Figure 1: Couette flow diagram. Frictional forces between the fluid and the plates result in the development of a non-uniform velocity profile.

and microfluidic suspensions are prepared using Newtonian fluids such as water or engine oil.

Particulate Suspensions

With the introduction of fine particles of some solid, the thermophysical properties of the system undergo significant change. In terms of flow behaviors, the velocity profile developed becomes disrupted by the presence of the particles, which move as rigid bodies with constant velocity. Returning to the case of Couette flow, this results in the altered velocity profile shown in Figure 2 (from [3] by permission). If the overall velocity gradient remains the same as before, the increased fluid velocity change in the areas between particles causes higher shear stress with the walls as well as between the fluid and the particles, thereby increasing the viscosity term.

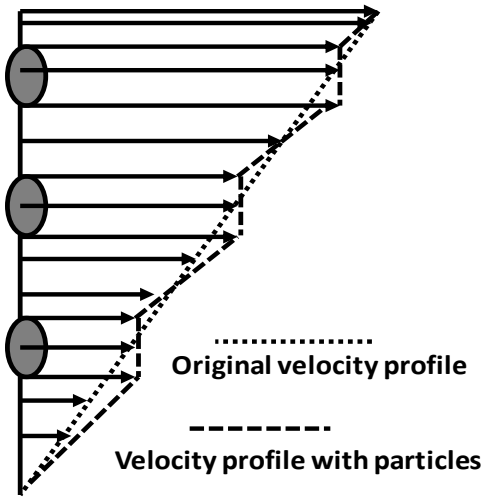

Figure 2: Couette flow of particulate suspension. The presence of particles disrupts the velocity profile of the fluid, causing higher shear stresses.

For nano- and microparticles, Brownian motion also contributes to an increase in viscosity. For large solids suspended within a flowing fluid, motion tends toward the direction of flow with little deviation. Although numerous individual fluid molecules are colliding with the solid particles from all directions, the net effect is minimal due to the comparatively negligible mass of the molecules. In the case of fine particles, however, these molecular collisions cause a significantly higher change in acceleration, with the result being a random motion of the particle known as Brownian motion. Figure 3 below

shows the simulated paths of several nanoparticles suspended within a fluid flow, with Brownian motion contributing greatly to the random

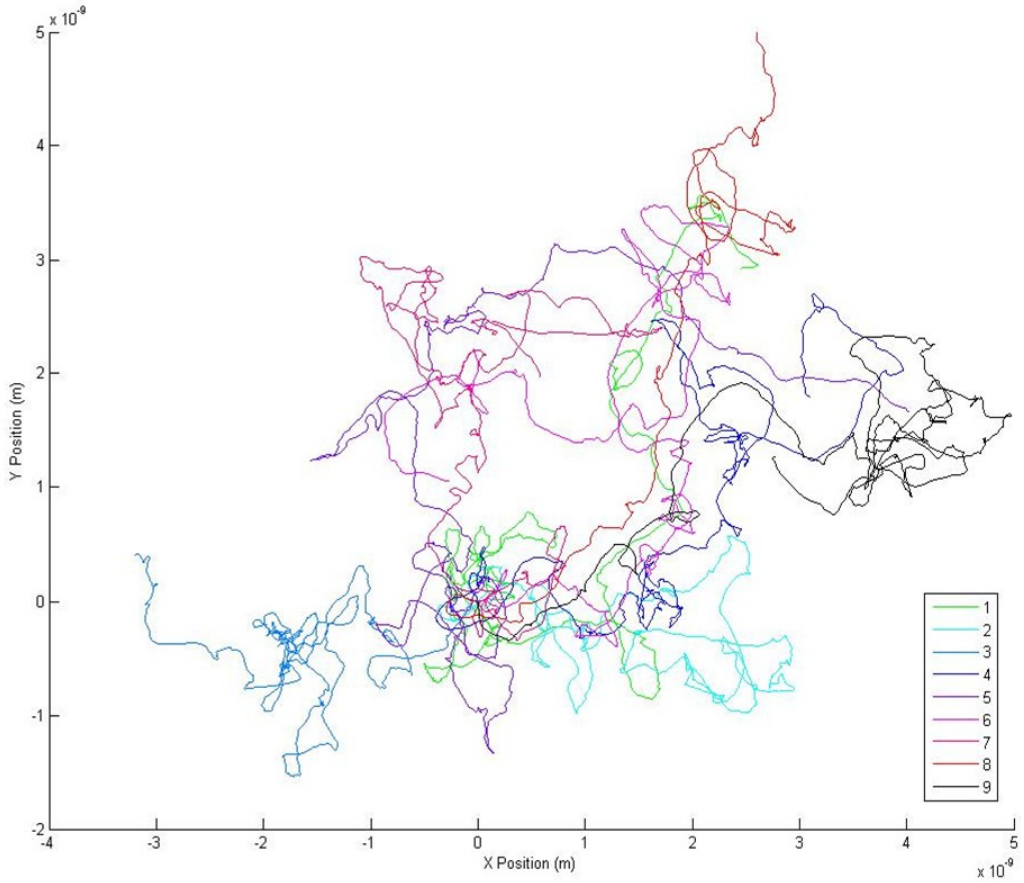

Figure 3: Nanoparticle motion as a result of Brownian forces. The simulation was performed using Al_2O_3 particles of 100nm in diameter, suspended in water. Though each particle started from the same position, randomized impacts with fluid molecules have caused significantly different trajectories.

trajectory of each particle. These additional components of particle motion increase the shear stresses at each solid-fluid boundary, further increasing viscosity.

Some attempts have been made to quantify the increase in viscosity as a result of introducing solid particles to a base fluid. The first was conducted by Einstein, who developed and later corrected an analytical model assuming a dilute suspension (ϕ<2%)

with spherical, non-interacting particles, resulting in the effective viscosity expression below:

$$\mu_e = \mu_f(1 + 2.5\phi) \quad . \tag{2}$$

A later study by Batchelor furthered this analysis by accounting for the effects of Brownian motion and hydrodynamic interactions between particles. He derived the following expression for suspensions of ϕ<10%:

$$\mu_e = \mu_f(1 + 2.5\phi + 6.25\phi^2) \quad . \tag{3}$$

Additional studies [4] with modified analyses have produced several forms of the Einstein and Batchelor expressions with different coefficients for the ϕ and ϕ^2 terms. Others have produced generalized empirical and analytical models accounting for dependencies on particle size and spacing, while yet more have developed empirical models for specific mixtures based on collected data. For the water-kaolinite mixtures in this study, empirical expressions for effective viscosity are derived using a modified form of the Einstein expression, with correlations for the ϕ coefficient, denoted by the function $K(T)$, developed in terms of temperature as shown below:

$$\mu_e = \mu_f(1 + K(T) * \phi) \quad . \tag{4}$$

EXPERIMENT

Equipment

Two capillary viscometers (Cannon-Fenske Routine Viscometers, Serial Numbers H138 and H268) were used to measure the effective viscosities of the water-kaolinite mixtures. Two viscometers were used during the experimental portion of this study for two reasons: 1) results could immediately be compared between viscometers as a means of identifying faulty tests; and 2) an average measurement for the two viscometers could

be used to reduce random error in the data. A larger group of viscometers were initially used in baseline testing of the viscosity of water; the H138 and H268 were chosen for further testing due to ease of use, as well as accuracy and consistency of results.

In order to measure viscosity across a range of temperatures, a constant-temperature water bath (PolyScience MX17VB6G-A11B, S/N 1A1420220) was utilized. Due to this model's lack of cooling coils, ice was used to artificially lower the bath temperature for tests below ambient temperature.

Other equipment used in this experiment include a magnetic stirrer (HANNA Instruments HI 200M, S/N A0006970) for suspension agitation; a triple beam balance for mass measurements; a pipette (Mohr, CE-PIPEG10, Home Science Tools) and a pipette pump (CE-PIPFL25, Home Science Tools) for charging and operating the viscometers; and a stopwatch.

Procedure

Each mixture was prepared by measuring the mass of an arbitrary volume of distilled water of approximately 200 mL, and using this value to calculate the necessary mass of kaolinite needed to produce a mixture with the desired volumetric ratio, according to the following equation, which stems from the principles of mass and conservation:

$$\phi = \frac{\frac{m_s}{\rho_s}}{\frac{m_s}{\rho_s} + \frac{m_f}{\rho_f}} \quad . \tag{5}$$

The kaolinite was then dispersed in the distilled water and agitated using the magnetic stirrer until proper suspension was achieved, usually requiring about 10 minutes, with up to 30 minutes for higher concentrations.

Using the pipette and pipette pump, each viscometer was filled with 4.4 mL of mixture, as suggested by manufacturer specification. The viscometers were then submerged in the water bath, held in place by viscometer holders, and the circulation of the bath was started. Once the bath temperature was reduced to 15 °C for the first measurement, approximately five minutes were allowed for the temperatures of the viscometers and mixture to equalize with the bath temperature. The viscometers remained suspended in the bath between subsequent tests, provided that they were operating normally; this eliminated the need for further delays for temperature equalization.

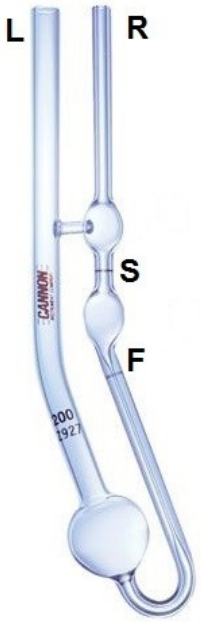

Figure 4: Viscometer diagram.

At each temperature, viscosity was tested using the same procedure for both viscometers. Referring to Figure 4, suction was applied to tube R using the pipette pump until the mixture was drawn into the reservoir above mark S. The vacuum was then released, and the time for the sample to flow from mark S to mark F was measured. By multiplying this efflux time by a specified constant for the viscometer, the kinematic viscosity was calculated. The dynamic viscosity was then calculated by multiplying the kinematic viscosity by the effective density of the mixture, found via the following equation:

$$\rho_e = \phi\rho_s + (1-\phi)\rho_f \quad . \tag{6}$$

Note that the value of ρ_e is different at each temperature point, as ρ_f decreases with increasing temperature, while ρ_s remains essentially constant.

Upon completion of testing for a given mixture, the viscometers were rinsed out with water and dried via paper towel. Lingering fluid in the capillary was forced into the

bulb reservoir by applying pressure to tube R with the pipette pump, allowing it to drain out.

RESULTS AND DISCUSSION

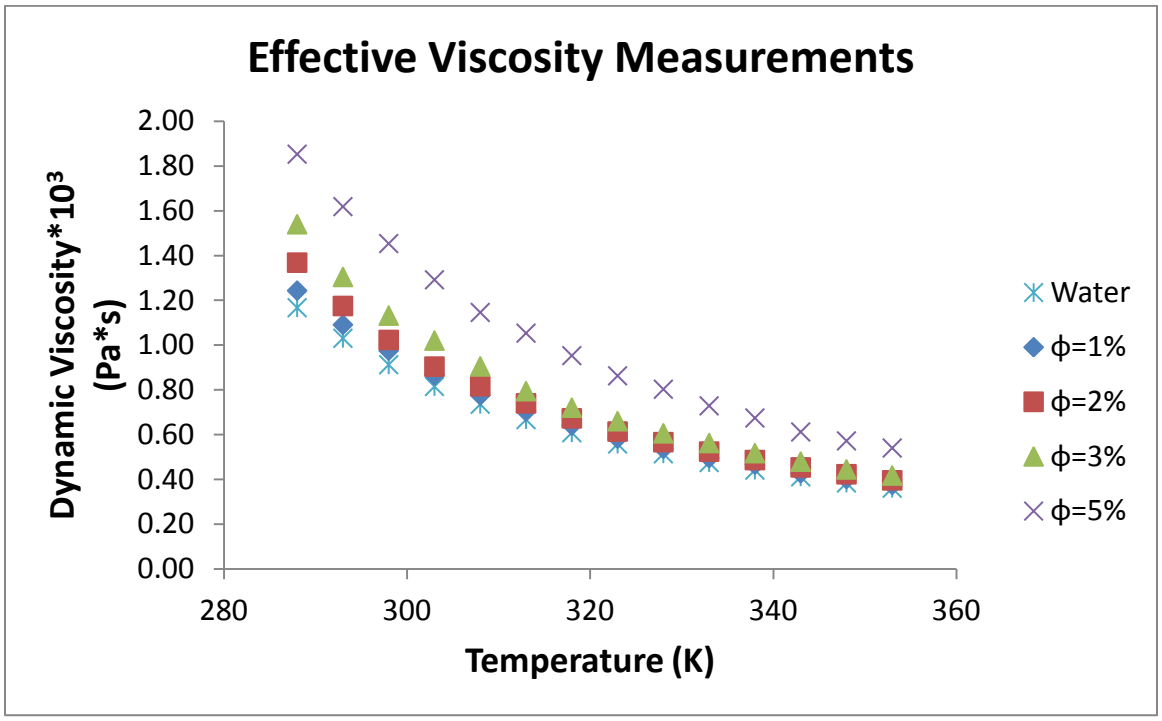

Figure 5: Measured effective viscosities of water-kaolinite mixtures.

Figure 5 above shows the results for effective viscosity of water-kaolinite mixtures at volumetric ratios of 1%, 2%, 3%, and 5%, as well as measurements for water only. Base testing of the viscosity of water was compared to established values in order to verify the performance of the viscometers. At each value of temperature, the percent difference between measured and published values for dynamic viscosity of water was less than 2.9%, with an average error of 2.16%. This error is within allowable limits for typical capillary viscometers.

Beginning with the base fluid (ϕ = 0%), Figure 5 shows that viscosity increases with increasing volumetric ratio at all temperatures. This trend agrees with the expected behavior of micro- and nanofluidic suspensions, as greater concentrations of particles

should create a greater disruption of the laminar velocity profile of the base fluid, as well as increase the shear stress associated with Brownian motion, thereby enhancing the viscosity of the mixture.

To determine if a correlation for $K(T)$ existed, the Einstein expression was rearranged in order to isolate $K(T)$. Equation (4) yields:

$$K(T) = \frac{\mu_e/\mu_f - 1}{\phi} \quad . \tag{7}$$

The value of $K(T)$ was then calculated for each data point using the measured values for μ_e and μ_f, and plotted as shown in Figure 6 below.

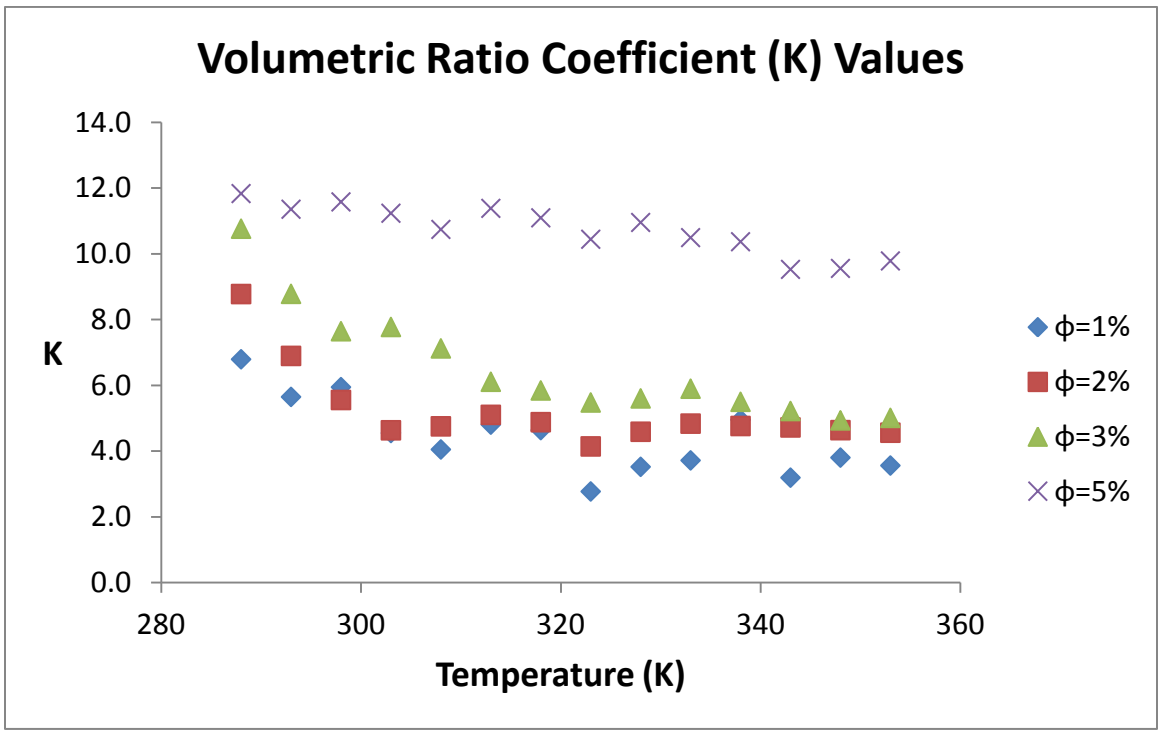

Figure 6: K values for measured viscosity data.

Analysis of these results shows what appears to be an exponential decay, with asymptotic behavior as T higher temperature values. Based on this observation, the proposed model for $K(T)$ is as follows:

$$K(T) = A[1 + Be^{-C(T-288)}] \quad . \quad (8)$$

A represents the asymptote of the model. As T grows very large, the term $e^{-C(T-288)}$approaches zero, reducing the entire equation to $K(T_{large}) = A$. The value for this coefficient was determined initially by sight and tuned as described below. B is determined by substituting the value of $K(288)$ into the equation and rearranging for B, as shown below:

$$B = \frac{K(288)}{A} - 1 \quad . \quad (9)$$

Following this, C can be evaluated by linearizing Equation 8 via the natural logarithm, as shown below:

$$\ln[K(T) - A] = \ln[\mathrm{AB}] - \mathrm{C}(\mathrm{T} - 288) \quad . \quad (10)$$

For each mixture, a graph of ln $[K(T) - A]$ versus $(T - 288)$ was plotted for the interval $288K \leq T \leq 313K$, as shown in Figure 7. A linear trendline was applied to each graph, the slope of which was taken as the value of $-C$. The linearized data for temperatures between 313K and 353K were rejected from these correlation graphs due to large deviations from the trendline. These deviations are a result of large values for the expression ln $[K(T) - A]$ caused by $K(T)$ approaching A, and are unverifiable due to limits in accuracy of the data.

Once initial values for A, B, and C were obtained for each of the four mixtures, these were substituted into Equation 8 and used to find percentage error between measured and calculated values of μ_e according to Equation 4. The constant A was then

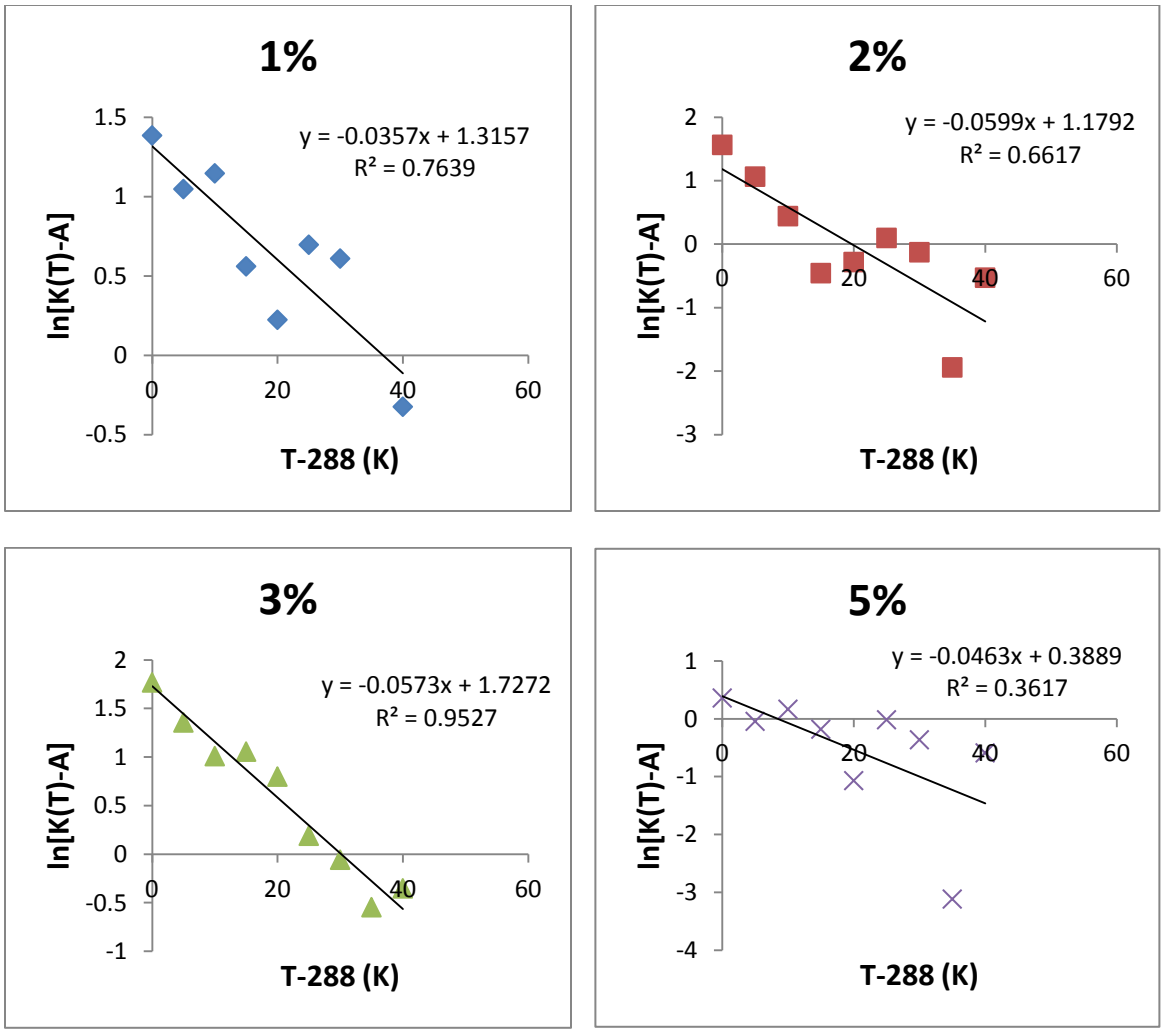

Figure 7: Correlation graphs for determining C.

tuned, with B and C subsequently modified, for each mixture with consideration to which value produced the lowest absolute average error, as well as the highest R^2 value in the correlation graphs for C. This process resulted in the final models displayed below in Table 1.

Table 1: Effective viscosity models for water-kaolinite suspensions	
1%	$\mu_e = \mu_f\left[1 + 2.8\phi\left(1 + 1.427e^{-0.0357(T-288)}\right)\right]$
2%	$\mu_e = \mu_f\left[1 + 4\phi\left(1 + 1.195e^{-0.0599(T-288)}\right)\right]$
3%	$\mu_e = \mu_f\left[1 + 4.9\phi\left(1 + 1.197e^{-0.0573(T-288)}\right)\right]$
5%	$\mu_e = \mu_f\left[1 + 10.4\phi\left(1 + 0.1379e^{-0.0357(T-288)}\right)\right]$

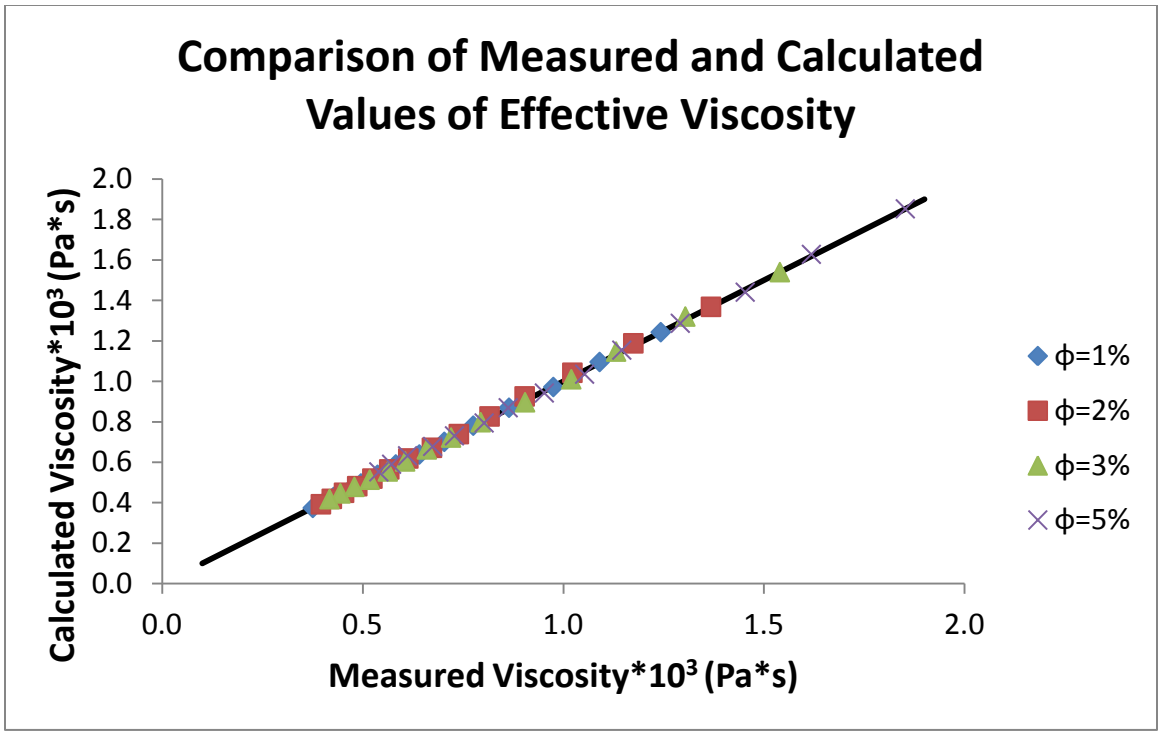

Figure 8: Comparison of measured and model-predicted viscosities.

To evaluate these models, the dynamic viscosity at each temperature and concentration measured was calculated using its respective model, and then compared to the original measured value. These results are shown in Figure 8 above, and percent differences between these values are tabulated in the appendix. The black line in Figure 8 shows a 1:1 correlation between measurement and calculation. The data points for each concentration fall neatly along this line, indicating that the models can accurately predict the effective viscosity of a water-kaolinite suspension within the given temperature and concentration ranges.

CONSIDERATIONS FOR ACCURACY OF RESULTS

As noted above, capillary viscometers typically have a measurement tolerance of 2-3%. Although care was taken to reduce the experimental error where possible, numerous factors still may have contributed to inaccuracies in the results. These factors

could include settling and separation of the suspensions, agglomeration of particles, and deposition of particles on the walls of the viscometer.

For the 1%, 2%, and 3% mixtures, the values which produced the lowest average error also resulted in an R^2 value at or near its maximum. For the 5% mixture, however, R^2 continued to increase as A decreased beyond a reasonable asymptotic value based on the data. This could be caused by the 5% mixture being at or beyond saturation, resulting in different behavior and the need for a different model than the mixtures of lower concentration.

Lastly, it is important to note that the empirically-derived expressions of Table 1 should not be used to extrapolate for values of $K(T)$ outside the temperature range and concentration range used in this experiment, as the rheological behavior of the suspension may differ unexpectedly at higher concentrations.

CONCLUSION

Without exception, the values of $K(T)$ measured were higher than the volumetric ratio coefficient of 2.5 in Einstein's revised effective viscosity model. As noted previously, Einstein's model assumes spherical particles, whereas particles of kaolinite are irregularly shaped. For the same volume of particles, this results in a greater total surface area, and subsequently larger shear forces at the liquid-solid boundary, thus increasing effective viscosity of the suspension. This observation likely holds true for industrial nanofluids, the particles of which tend to be irregularly shaped due to the processes used to form them. Furthermore, other experimental studies into nanofluid viscosity have all measured constants greater than Einstein's suggested 2.5 [5,6]. It is of

great importance, therefore, that viscosity of particulate suspensions be studied in more detail in order to better define these behaviors.

Further Research

At the time of writing, the above correlations have only been verified for water-kaolinite mixtures at the measured temperatures and volumetric ratios. It is planned to perform additional testing of mixtures of water and diatomaceous earth and to determine whether or not similar correlations and trends are present. Should these results match well with the results of this experiment, further testing will be performed on other mixtures, including those with mixtures of two or more types of particles. It is hoped that a general model for nano- and microfluidic suspensions with irregularly shaped particles can be developed from these tests.

APPENDIX: EXPERIMENTAL DATA

Viscosity Test Data

	Dynamic Viscosity*10^3 (Pa*s)				
Temp. (K)	Dist. Water	φ=1%	φ=2%	φ=3%	φ=5%
288	1.1672	1.2431	1.3684	1.5400	1.8528
293	1.0303	1.0907	1.1747	1.3044	1.6186
298	0.9125	0.9753	1.0228	1.1317	1.4536
303	0.8151	0.8648	0.9038	1.0201	1.2918
308	0.7356	0.7756	0.8163	0.9048	1.1459
313	0.6671	0.7035	0.7397	0.7943	1.0533
318	0.6086	0.6413	0.6727	0.7203	0.9529
323	0.5581	0.5825	0.6138	0.6600	0.8628
328	0.5145	0.5370	0.5663	0.6059	0.8028
333	0.4752	0.4957	0.5242	0.5626	0.7288
338	0.4417	0.4661	0.4864	0.5174	0.6744
343	0.4119	0.4277	0.4536	0.4794	0.6119
348	0.3841	0.4018	0.4230	0.4444	0.5721
353	0.3607	0.3757	0.3958	0.4173	0.5402

Measured Values of $K(T)$

Temp. (K)	φ=1%	φ=2%	φ=3%	φ=5%
288	6.7944	8.7785	10.7668	11.8345
293	5.6497	6.8962	8.7850	11.3581
298	5.9464	5.5555	7.6475	11.5820
303	4.5512	4.6337	7.7771	11.2361
308	4.0505	4.7542	7.1250	10.7441
313	4.8067	5.1033	6.1103	11.3850
318	4.6394	4.8806	5.8456	11.0970
323	2.7737	4.1435	5.4799	10.4445
328	3.5230	4.5898	5.6040	10.9559
333	3.7181	4.8372	5.8997	10.4949
338	4.9532	4.7648	5.5005	10.3704
343	3.1934	4.7210	5.2205	9.5289
348	3.8038	4.6379	4.9360	9.5578
353	3.5616	4.5603	5.0117	9.7856

Percent Difference Between Measured Viscosities and Viscosities Predicted by Models in Table 1

Percent Difference (%)				
Temperature (K)	φ=1%	φ=2%	φ=3%	φ=5%
288	0.00	0.00	0.00	0.00
293	0.46	1.13	1.23	0.57
298	0.33	1.91	1.36	0.89
303	0.56	2.37	0.96	0.38
308	0.68	1.25	0.89	0.73
313	0.35	0.06	0.48	1.72
318	0.45	0.16	0.27	1.10
323	1.13	0.82	0.54	0.78
328	0.23	0.28	0.29	1.07
333	0.11	0.94	1.42	0.27
338	1.42	0.96	0.69	0.56
343	0.16	1.00	0.18	3.28
348	0.52	0.93	0.40	3.10
353	0.36	0.85	0.08	2.27

REFERENCES

[1] Taylor, R., Coulombe, S., Otanicar, T., Phelan, P., Gunawan, A., Lv, W., . . . Tyagi, H. (2013). Small particles, big impacts: A review of the diverse applications of nanofluids. *Journal of Applied Physics, 113*(1), 3/15/15.

[2] Munson, B. R., Young, D. F., Okiishi, T. H. (2002). *Fundamentals of fluid mechanics* (7th ed.) John Wiley and Sons.

[3] Michaelides, E. (2014). *Nanofluidics: Thermodynamic and transport properties* (1st ed.) Springer International Publishing.

[4] Mishra, P. C., Mukherjee, S., Nayak, S. K., Panda, A. (2014). A brief review on viscosity of nanofluids. *International Nano Letters, 4*(4), 3/25/15.

[5] Chen, H., Ding, Y., He, Y., Tan, C. (2007). Rheological behaviour of ethylene glycol based titania nanofluids. *Chem. Phys. Lett., 444*(4-6), 3/25/15.

[6] Pak, B. C., Cho, Y. I. (1998). Hydrodynamic and heat transfer study of dispersed fluids with submicron metallic oxide particles. *Exp. Heat Transf Int. J., 11*(2), 3/25/15.